Bioconjugate Chemistry

Communication

pubs.acs.org/bc

Targeted Molecular Imaging of Cancer Cells Using MS2-Based ^{129}Xe NMR

Keunhong Jeong,[†,‡] Chawita Netirojjanakul,[†] Henrik K. Munch,[†] Jinny Sun,[†] Joel A. Finbloom,[†] David E. Wemmer,[†,§] Alexander Pines,[†,‡] and Matthew B. Francis*[,†,‡]

[†]Department of Chemistry, University of California, Berkeley, California 94720-1460, United States

[‡]Materials Sciences Division and [§]Physical Biosciences Division, Lawrence Berkeley National Laboratory, Berkeley, California 94720-1460, United States

Supporting Information

ABSTRACT: We have synthesized targeted, selective, and highly sensitive ^{129}Xe NMR nanoscale biosensors using a spherical MS2 viral capsid, Cryptophane A molecules, and DNA aptamers. The biosensors showed strong binding specificity toward targeted lymphoma cells (Ramos line). Hyperpolarized ^{129}Xe NMR signal contrast and hyper-CEST ^{129}Xe MRI image contrast indicated its promise as highly sensitive hyperpolarized ^{129}Xe NMR nanoscale biosensor for future applications in cancer detection in vivo.

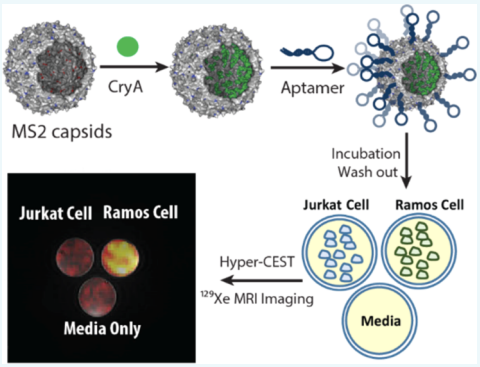

INTRODUCTION

Magnetic resonance imaging (MRI) is a highly useful medical imaging tool, affording high-resolution images with minimal invasiveness. This well-established technique generally detects the protons of water and lipids in the body, which provides flexible and detailed anatomical imaging due to the high abundance of these molecules. However, the imaging of specific, nonabundant molecules of interest, such as cancer biomarkers, is significantly limited by the low signal-to-noise ratio that can be achieved against the background of ubiquitous water molecules. In these cases other nuclei can be imaged, but the low polarization under normal conditions limits both detection levels and dynamic range. To overcome these problems, various techniques have been developed to enhance signal intensity and sensitivity, and these are often combined with molecular sensors to generate localized contrast with high chemical specificity. In particular, hyperpolarization by spin exchange optical pumping (SEOP) and dynamic nuclear polarization (DNP) have been highlighted as methods to increase polarization, and hence imaging sensitivity, which is particularly important for nuclei other than protons.[1,2]

^{129}Xe is an ideal reporter for NMR because it is inert, hyperpolarizable, and biocompatible, and provides no natural background signal in living systems.[3,4] The use of hyperpolarized ^{129}Xe as an imaging agent has been demonstrated in the magnetic resonance imaging of lung tissue,[5,6] brain,[7,8] and kidneys.[9] For molecular imaging, Cryptophane A (CryA) based xenon sensors have been developed with chemical exchange saturation transfer (CEST) to increase the detection sensitivity by 1000- to 1 million-fold relative to the direct observation of the caged xenon.[3,10−12] In addition, cucurbit[6/7]urils have recently been reported as xenon sensors.[13−15] Molecular sensors carrying large numbers of CryA moieties coupled to targeting groups provide a further increase in sensitivity, and have been applied to the detection of cancer cells. Hyper-CEST NMR imaging with these multivalent CryA sensors may thus provide powerful tools for the detection of molecular targets—especially those on cancer cells for which early-stage detection is highly critical for patient survival.[16]

Along with several recent reports of carrier structures bearing sensing groups,[17−19] previous studies in our groups have found that bacteriophage MS2 has a long circulation half-life in vivo,[20] and is a promising water-soluble scaffold for encapsulating hydrophobic CryA entities. Key to its success is the presence of 32 2-nm pores in the 27-nm-diameter protein shell, which provide rapid access of small reagents and Xe into the internal volume. This allows over 100 CryA molecules to be housed inside the sphere in a manner that avoids losses of water solubility that would otherwise be expected if those were attached externally.[21] Our previous studies with this MS2-CryA construct were limited to untargeted carriers that could not engage specific cells.[22] More recently, filamentous phage with genetically encoded single chain antibody (scFv) groups were used to distinguish between different cell types based on their

Received: May 31, 2016
Revised: July 13, 2016

DOI: 10.1021/acs.bioconjchem.6b00275
Bioconjugate Chem. XXXX, XXX, XXX−XXX

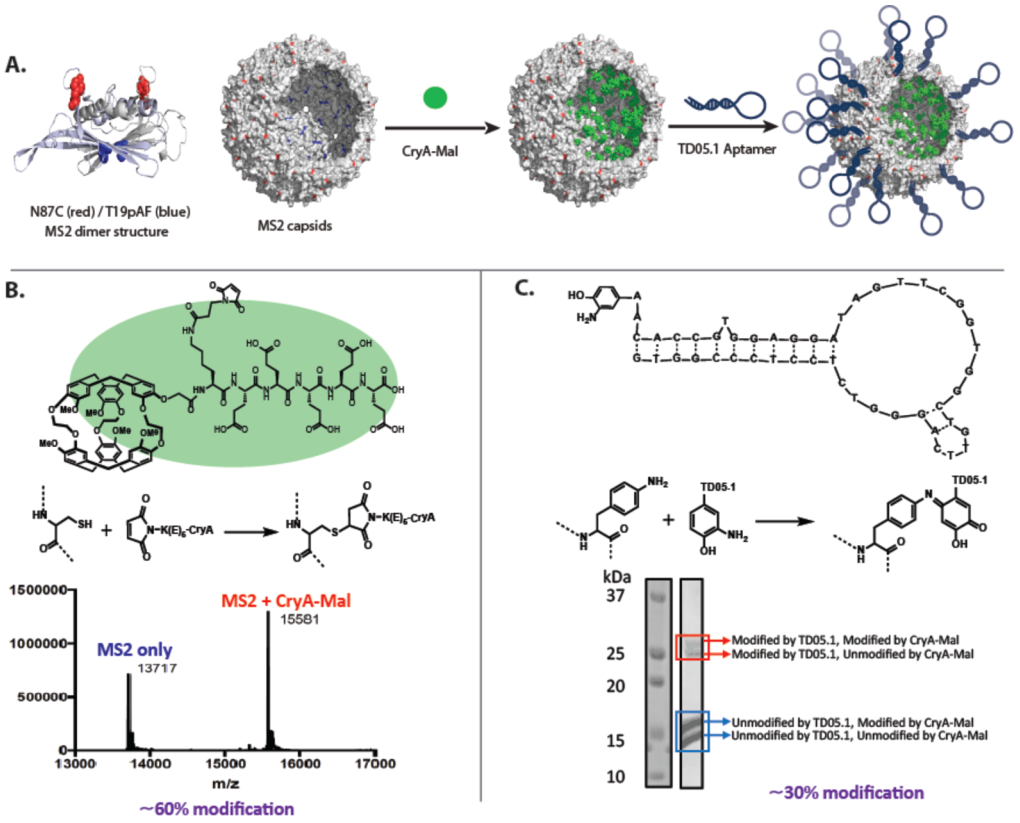

Figure 1. Scheme of ^{129}Xe-biosensor synthesis and identification. (A) The MS2 viral capsid (PDB ID: 2MS2[30]) was modified with CryA-Mal (indicated by the green circle, with the structure shown in B) at ~110 N87C positions on the interior surface of the capsid. This was followed by the attachment of 54 aminophenol-TD05.1 aptamers to T19*p*AF residues on the exterior surface. (B) Interior thiol-maleimide reactions on the N87C positions with the CryA-Linker shown (20 equiv CryA, pH 7.2 phosphate buffer, rt, 6 h) resulted in the modification of 60% of the available cysteines, as determined using ESI-TOF MS. (C) Exterior oxidative coupling reactions on T19*p*AF residues with TD05.1 DNA-aminophenol molecules (10 equiv aminophenol-TD05.1 aptamer, 25 equiv $NaIO_4$, pH 6.5 phosphate buffer, rt, 5 min) led to the modification of 30% of the capsid proteins, as determined using SDS-PAGE and densitometry analysis after Coomassie staining.

surface markers. In that study, the CryA groups were installed on the external surfaces of the carriers, accompanied by over 1000 molecules of polyethylene glycol (PEG) to maintain solubility and prevent aggregation.

The need for solubilizing PEG coatings limits the potential for the orthogonal attachment of targeting moieties. An optimized carrier would combine aspects of both designs, integrating the dense sphere of CryA molecules housed inside MS2, with large numbers of external targeting groups through a modular coupling strategy. Here we report the generation and evaluation of such a system, providing both a high payload of internal CryA groups and external targeting aptamers for the highly sensitive detection of lymphoma cells.

RESULTS AND DISCUSSION

The MS2 protein monomers used in this study were engineered with N87C mutations, which created a series of 180 sulfhydryl groups facing the interior surface of each capsid following assembly.[23] To enable the use of oxidative coupling strategies for the introduction of targeting moieties on the external surfaces,[23,24] *p*-aminophenylalanine (*p*AF) residues were also incorporated into position 19 of each monomer (resulting in 180 per assembled capsid) using the Schultz amber suppression technique.[23−25] The interior of the N87C-T19*p*AF capsids was first modified with CryA-maleimide (CryA-Mal) (Figure 1B). To increase the solubility of the conjugate during the conjugation step, five glutamic acids were incorporated into the CryA-Mal linker, which was prepared with solid-phase peptide synthesis (SPPS) (Figure 1B and Supporting Information Figure S1). ESI-TOF-MS analysis of the MS2 coat protein after coupling with 20 equiv of CryA-Mal and disassembly revealed that about 60% of the monomers had been modified, corresponding to an average of 110 CryA molecules per intact capsid (Figure 1B). Modification with fewer equivalents of CryA-Mal was attempted with lower modification levels. In a separate set of capsids, the cysteine residues were labeled with Oregon Green maleimide to allow their detection in flow cytometry experiments. Virtually complete labeling of the 180 cysteine residues was achieved in this case (Supporting Information Figure S2).

We chose DNA aptamers as targeting agents due to evolvable specificity and affinity for tumor cell biomarkers.[26] The exterior of MS2 was modified with the TD05.1 aptamer, which targets membrane-bound mIgM markers expressed on lymphoma cells.[27,28] The DNA aptamers were modified with aminophenol groups at the 5′-termini, allowing them to be conjugated to the aniline side chains of the *p*AF residues via oxidative coupling in the presence of sodium periodate.[23,27,29] SDS-PAGE analysis indicated that approximately 30% of the 180 monomers were derivatized with oligonucleotides, which resulted in significant gel shifts (Figure 1C). Additionally, the addition of the CryA groups to the MS2 monomers resulted in the appearance of slower migrating bands that corresponded to both the unmodified and the DNA-conjugated proteins (Figure 1C).

DOI: 10.1021/acs.bioconjchem.6b00275
Bioconjugate Chem. XXXX, XXX, XXX−XXX

To verify the ability of the doubly modified MS2 capsids to target cancer cells, fluorescent versions of the capsids (Supporting Information Figure S2) were exposed to Ramos Burkitt's lymphoma cells, which are positive for the mIgM marker. Following 1 h of exposure on ice, flow cytometry analysis indicated strong binding of the TD05.1-labeled capsids to the targeted cells (Figure 2). A small population of cells showed minimal capsid binding. This is likely due to the lack of mIgM markers on some cells. As a negative control, the TD05.1-labeled capsids were also exposed to Jurkat cells, which are a T-cell leukemia line that lacks the mIgM groups. In this case, only a minor increase in fluorescence was observed upon flow cytometry analysis (Figure 2). In addition, negative aptamer control (MS2-sgc8c) test was carried out on Ramos cell and it showed no strong binding result (Figure S6). Taken together, these experiments indicate that the capsid-bound aptamer interaction remains specific for the mIgM group.

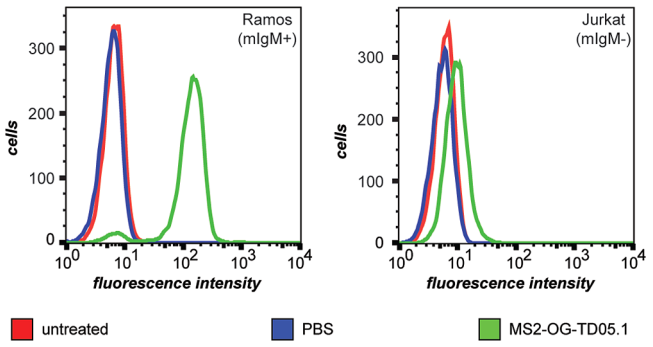

Figure 2. Binding specificity analysis of MS2-TD05.1 conjugates. The MS2 viral capsids were fluorescently labeled with Oregon Green maleimide dyes at the interior N87C positions, followed by modification with aminophenol-TD05.1 aptamers at the T19*p*AF sites on the exterior. The MS2-OG-TD05.1 constructs were then incubated with Ramos (mIgM$^+$) and Jurkat (mIgM$^-$) cells on ice for 1 h. Flow cytometry analysis indicated that the MS2-OG-TD05.1 agents bound to the Ramos target cells but not the Jurkat cells.

The ability of the capsids to report the presence of the targeted biomarker using ^{129}Xe Hyper-CEST NMR was next demonstrated using the same aptamer sequence. MS2-CryA-TD05.1 conjugates were incubated with a sample of 2×10^7 Ramos or Jurkat cells in 0.5 mL of a binding buffer that contained 4.5 g/L glucose, 5 mM $MgCl_2$, 1% BSA, and 0.1 mg/mL yeast tRNA (see Methods and Materials for details) for 1 h on ice. Unbound MS2 was then removed using three washes and cells were transferred to RPMI media (RPMI 1640, containing 10% fetal bovine serum, 2 mM L-glutamine, 100 μg/mL streptomycin, and 100 U/mL penicillin) containing 0.2% L-81 as a detergent to suppress foaming. Hyperpolarized ^{129}Xe gas was flowed through a tube from the polarizer to the solution of cells. Hyper-CEST detection was employed by applying a selective-bandwidth saturation pulse (dSNOB) and monitoring the degree of saturation transfer. A broad Xe@CryA peak was identified at 57 ppm (which is consistent with previous observations)[21] in the Ramos cell sample (Figure 3A).

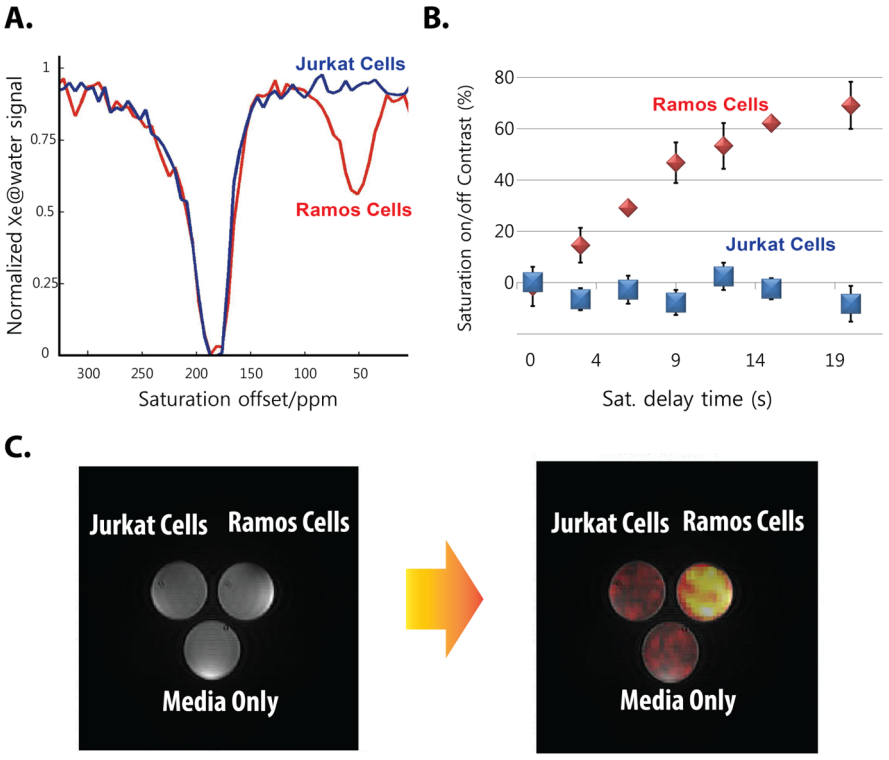

Figure 3. NMR/MRI experiments with cell suspension samples. The MS2-CryA-TD05.1 agents (167 nM in capsids) were incubated with 2×10^7 Ramos or Jurkat cells for 1 h on ice. Following this, the cells were washed three times to remove unbound biosensors. The cells were resuspended in 500 μL of media for NMR/MRI analysis. (A) Hyper-CEST spectra corresponding to Ramos and Jurkat cell samples. The data indicate that MS2 biosensors only remain bound in the Ramos samples. (B) On vs off saturation contrast values were measured for different saturation times using the two cell samples. (plots with contrast ± standard deviation for four replicates). (C) Hyper-CEST saturation MRI contrast images clearly distinguished the receptor-positive cell sample (left, proton image; right, Hyper-CEST ^{129}Xe image overlapped onto the proton image). The contrast color scale bar is included in the SI.

DOI: 10.1021/acs.bioconjchem.6b00275
Bioconjugate Chem. XXXX, XXX, XXX−XXX

In contrast, this peak was entirely absent in the Jurkat sample. This indicated that the targeted capsids were capable of distinguishing between the cell populations, as observed in the flow cytometry experiments.

A contrast diagram was produced by comparing the off-resonance and on-resonance saturation signals for each cell solution as a function of saturation time (Figure 3B). The result again confirmed the presence of biosensors only in the Ramos cell population. Increasing saturation time was found to enhance the contrast and thus provide higher detection sensitivity, ultimately reaching a contrast difference of 69.1 ± 9.2% with a 20 s saturation duration.

To explore the potential of the capsid carriers as targeted MR imaging agents, a ^{129}Xe hyper-CEST saturation MRI contrast map[31] was obtained by comparing the off-resonance and on-resonance images for a sample comprising three tubes: media only, media with Jurkat cells, and media with Ramos cells (Figure 3C). The two cell-containing samples were exposed to the MS2-CryA-TD05.1 agents as described above. An 8 s saturation time was used in this experiment (saturation condition for obtaining ∼50% contrast difference was used). As expected there was no contrast in the media and Jurkat tubes. However, strong contrast was generated for the Ramos cell sample. This result demonstrates that the capsid-based nanocarriers can indeed report biologically relevant levels of a specific biomarker in an MR image.

CONCLUSIONS

The in vivo use of xenon MRI has been studied previously.[32,33] The saturation time that can be applied is largely determined by the ^{129}Xe relaxation time (T1), which is about 20 s in lung tissue and 4−13 s in dissolved oxygenated blood.[34,35] Furthermore, Mugler et al.[36] observed that the transit time of dissolved ^{129}Xe from lung to brain in humans by blood flow is 5 s. A recent study with modified MS2 showed that more than 8% was distributed in the rat lung 24 h post-dosage, and more than 20% of the injected MS2 remained in the blood.[20] Further, MS2 has demonstrated no cell toxicity in extensive in vitro studies.[37,38] Together, these findings suggest that hyperpolarized xenon transfer in the lung will provide sufficient signal for detection of specific cancer cells targeted with the MS2-CryA conjugates in MRI images.

Here we describe the synthesis of a high-sensitivity MS2-based ^{129}Xe NMR nanoscale sensor that selectively recognizes cancer cells. The biosensor prepared was designed to target a lymphoma cell line; however, the attachment of other aptamers, peptides, or antibodies to the exterior of MS2 is straightforward due to the flexibility of the oxidative coupling strategy. This suggests broad applicability of this construct as in vivo explorations commence. We have also demonstrated the advantage of the internal CryA functionalization strategy for increasing agent sensitivity, in conjunction with ^{129}Xe Hyper-CEST. Importantly, along with recent extensive ^{129}Xe sensitive biomaterial development,[32,33] this work provides a strong basis for the continued exploration of targeted cancer cell imaging agents with future applications in NMR and MRI.

MATERIALS AND METHODS

MS2 Capsid−TD05.1 Biding Assays. Flow cytometry was used to determine binding ability of all of the MS2−aptamer constructs. For all samples, 100 μL of 2 × 10^6 cells/mL of Ramos or Jurkat cells were used, suspended in binding buffer (4.5 g/L glucose, 5 mM $MgCl_2$, 0.1 mg/mL yeast tRNA (Sigma), and 1 mg/mL BSA (Fisher) in Dulbecco's PBS with calcium chloride and magnesium chloride (Invitrogen)). To these cells were added 10 μL of 6 μM MS2-OG-TD05.1 construct solutions (MS2-OG monomer concentration, Supporting Information Figure S2). The samples were then incubated on ice for 1 h. The resulting cells were washed twice with 500 μL of binding buffer and resuspended in 200 μL of binding buffer. The cells were analyzed by flow cytometry (FACSCalibur flow cytometer, BD Biosciences) to determine the amount of Oregon Green fluorescence. For each sample, 10,000 cells were counted.

Analyzing Biosensor by ^{129}Xe NMR. A gas mixture (2% ^{129}Xe natural abundance, 10% N_2, 88% He) was hyperpolarized via spin-exchange optical pumping (SEOP) using a home-built polarizer.[34] After polarization, the gas was routed directly to a 5 mm NMR tube. ^{129}Xe was dissolved into the sample solution via bubbling through a capillary running down to the bottom of the NMR tube at a rate of 0.4 SLM for 10 s. Total gas pressure was maintained at 2.38 atm. The bubbling period was followed by a 4 s wait period to allow the solution to settle. All ^{129}Xe NMR data were acquired on a 400 MHz (9.4 T) Varian VNMRS console. Spectra were acquired with 30.5 kHz spectral width in 1 s. ^{129}Xe NMR was carried out with 40 million cells mL^{-1} concentration of Ramos cells and Jurkat cells, respectively. After rinsing out unbound biosensors, the saturation profile of each sample was measured by recording the Xe@water signal as a function of the RF pulse frequency train. Twenty million cells in 500 μL media buffer of Ramos cells and Jurkat cells were prepared for the NMR experiment. Ramos and Jurkat cells were spun down and resuspended in 4 mL of binding buffer to a final cell density of 5 × 10^6 cells/mL. The cell solution was mixed with 400 μL of 30 μM MS2-CryA-TD05.1 construct solutions and incubated on ice for 1 h with constant shaking. The cells were then washed twice with 10 mL binding buffer and washed once with 10 mL NMR media (RPMI 1640 supplemented with 1% P/S, 1% L-Gln, and 0.02% L-81). The cells were then resuspended in 500 μL NMR media for the NMR experiment. dSNOP pulses[22,35] with 500 Hz bandwidth were used with the same pulse sequence previously used,[22,36] except the saturation time was 8 s (Figure 3A). Contrasts with different saturation time were measured with saturation on and off pulses (6300 Hz and 35,900 Hz) four times with 0, 3, 6, 9, 12, 15, and 20 s, respectively (Figure 3B).[39] For ^{129}Xe Hyper-CEST saturation MRI, we used a custom phantom comprising of three 5-mm NMR tubes packed into a triangular configuration. This custom phantom could fit inside of a 10 mm NMR probe. Each tube had an individual gas capillary. Xenon images were acquired using a modified fast spin−echo imaging sequence that included bubbling and waiting times, as well as a saturation pulse prior to excitation as previously used.[22] Total gas pressure was maintained at 2.44 atm and the flow rate was 0.4 SLM. The solution was typically bubbled for 10 s followed by a 6 s wait. The dSNOB pulse was 6.5 μs, a train of 4 echoes was used with an echo time of 10 ms, and the overall repetition time (TR) was 22.5 s. Signals were acquired with a 12.02 kHz spectral width and 2.66 ms acquisition time. All images were acquired in the axial orientation using 16 averages. The field of view was 20 mm by 20 mm. Xenon images had a *k*-space matrix of dimensions 32 readout by 32 phase encode points. A ^{129}Xenon contrast map (Supporting Information Figure S3-c) was obtained using custom MATLAB scripts that apodized the signal using a 10 Hz

DOI: 10.1021/acs.bioconjchem.6b00275
Bioconjugate Chem. XXXX, XXX, XXX−XXX

exponential function. The *k*-space of off-resonance (Figure S3-b) was subtracted from the on-resonance (Figure S3-a) saturation images voxel-by-voxel. The subtracted image was then normalized by dividing it by the off-saturation image (Figure S3-c). The regions of interest defined by the proton image (Figure S3-d) was used to make the final ^{129}Xe contrast map (Figure S3-e). Significant ^{129}Xe contrast was only obtained in the Ramos cell solution. MS2 capsid intactness after Xenon bubbling was proved with dialysis using spin concentrator (Supporting Information 7). The status of cells in sample might be influenced by the experimental pressure or xenon bubbling. However, this proof-of-principle experiment demonstrated that this MS2 biosensor had a selective binding on the surfaces of live cells.

The proton image was obtained using a fast spin−echo imaging sequence (TR = 1.5 s, TE = 16.7 ms, 4 echoes per excitation) after 2 ms excitation. The *k*-space matrix dimension was 192 points in both readout and phase encode dimensions. The field of view was 20 mm by 20 mm. Signals were acquired with a 20.16 kHz spectral width and 9.52 ms acquisition time. All proton images were acquired using 4 averages.

■ ASSOCIATED CONTENT

Supporting Information

The Supporting Information is available free of charge on the ACS Publications website at DOI: 10.1021/acs.bioconjchem.6b00275.

Experimental procedures and materials (PDF)

■ AUTHOR INFORMATION

Corresponding Author

*E-mail: mbfrancis@berkeley.edu.

Notes

The authors declare no competing financial interest.

■ ACKNOWLEDGMENTS

We would like to thank Dr. R. Matthew Ramirez and Ioana L. Aanei for valuable discussions. C.N. was supported by a HHMI International Student Research Fellowship and H.M. was supported by the Villum Kann Rasmussens Foundation and the Laboratory Directed Research and Development Program at Lawrence Berkeley National Laboratories. K.J. and C.N. were also supported by the Berkeley Chemical Biology Graduate Program (NIH Training Grant 1 T32 GMO66698) during research rotations. J.A.F. was supported by the Department of Defense through the National Defense Science and Engineering Graduate Fellowship. This work was supported by the U.S. Department of Energy, Office of Science, Basic Energy Sciences, Materials Sciences and Engineering Division, under Contract No. DE-AC02-05CH11231.

■ REFERENCES

(1) Lee, H., Sun, E., Ham, D., and Weissleder, R. (2008) Chip-NMR biosensor for detection and molecular analysis of cells. *Nat. Med. 14*, 869−874.

(2) Lee, Y. J., Park, K.-D., Huang, S.-J., Liu, S.-B., and Lee, H.-J. (2007) Characterization of nanoporous structures of polyphenylene oxide derived carbon membranes by means of ^{129}Xe NMR. *J. Nanosci. Nanotechnol. 7*, 3932−3937.

(3) Schröder, L., Lowery, T. J., Hilty, C., Wemmer, D. E., and Pines, A. (2006) Molecular imaging using a targeted magnetic resonance hyperpolarized biosensor. *Science 314*, 446−9.

(4) Schröder, L. (2013) Xenon for NMR biosensing–inert but alert. *Phys. Med. 29*, 3−16.

(5) Driehuys, B., Cofer, G. P., Pollaro, J., Mackel, J. B., Hedlund, L. W., and Johnson, G. A. (2006) Imaging alveolar-capillary gas transfer using hyperpolarized ^{129}Xe MRI. *Proc. Natl. Acad. Sci. U. S. A. 103*, 18278−83.

(6) Stewart, N. J., Norquay, G., Griffiths, P. D., and Wild, J. M. (2015) Feasibility of human lung ventilation imaging using highly polarized naturally abundant xenon and optimized three-dimensional steady-state free precession. *Magn. Reson. Med. 74*, 346−52.

(7) Mazzanti, M. L., Walvick, R. P., Zhou, X., Sun, Y., Shah, N., Mansour, J., Gereige, J., and Albert, M. S. (2011) Distribution of hyperpolarized xenon in the brain following sensory stimulation: preliminary MRI findings. *PLoS One 6*, e21607.

(8) Swanson, S. D., Rosen, M. S., Agranoff, B. W., Coulter, K. P., Welsh, R. C., and Chupp, T. E. (1997) Brain MRI with laser-polarized ^{129}Xe. *Magn. Reson. Med. 38*, 695−698.

(9) Swanson, S. D., Rosen, M. S., Coulter, K. P., Welsh, R. C., and Chupp, T. E. (1999) Distribution and dynamics of laser-polarized ^{129}Xe magnetization in vivo. *Magn. Reson. Med. 42*, 1137−1145.

(10) Kunth, M., Döpfert, J., Witte, C., Rossella, F., and Schröder, L. (2012) Optimized use of reversible binding for fast and selective NMR localization of caged xenon. *Angew. Chem., Int. Ed. 51*, 8217−8220.

(11) Schröder, L., Meldrum, T., Smith, M., Lowery, T., Wemmer, D., and Pines, A. (2008) Temperature Response of ^{129}Xe Depolarization Transfer and Its Application for Ultrasensitive NMR Detection. *Phys. Rev. Lett. 100*, 257603.

(12) Bai, Y., Hill, P. A., and Dmochowski, I. J. (2012) Utilizing a water-soluble cryptophane with fast xenon exchange rates for picomolar sensitivity NMR measurements. *Anal. Chem. 84*, 9935−41.

(13) Finbloom, J. A., Slack, C. C., Bruns, C. J., Jeong, K., Wemmer, D. E., Pines, A., and Francis, M. B. (2016) Rotaxane-mediated suppression and activation of cucurbit[6]uril for molecular detection by ^{129}Xe hyperCEST NMR. *Chem. Commun. (Cambridge, U. K.) 52*, 3119−22.

(14) Schnurr, M., Sloniec-Myszk, J., Döpfert, J., Schröder, L., and Hennig, A. (2015) Supramolecular Assays for Mapping Enzyme Activity by Displacement-Triggered Change in Hyperpolarized ^{129}Xe Magnetization Transfer NMR Spectroscopy. *Angew. Chem., Int. Ed. 54*, 13444−13447.

(15) Kunth, M., Witte, C., Hennig, A., and Schröder, L. (2015) Identification, classification, and signal amplification capabilities of high-turnover gas binding hosts in ultra-sensitive NMR. *Chem. Sci. 6*, 6069−6075.

(16) Taratula, O., and Dmochowski, I. J. (2010) Functionalized ^{129}Xe contrast agents for magnetic resonance imaging. *Curr. Opin. Chem. Biol. 14*, 97−104.

(17) Klippel, S., Freund, C., and Schröder, L. (2014) Multichannel MRI Labeling of Mammalian Cells by Switchable Nanocarriers for Hyperpolarized Xenon. *Nano Lett. 14*, 5721−5726.

(18) Schnurr, M., Sydow, K., Rose, H. M., Dathe, M., and Schröder, L. (2015) Brain Endothelial Cell Targeting Via a Peptide-Functionalized Liposomal Carrier for Xenon Hyper-CEST MRI. *Adv. Healthcare Mater. 4*, 40−45.

(19) Stevens, T. K., Ramirez, R. M., and Pines, A. (2013) Nanoemulsion Contrast Agents with Sub-picomolar Sensitivity for Xenon NMR. *J. Am. Chem. Soc. 135*, 9576−9579.

(20) Farkas, M. E., Aanei, I. L., Behrens, C. R., Tong, G. J., Murphy, S. T., O'Neil, J. P., and Francis, M. B. (2013) PET Imaging and Biodistribution of Chemically Modified Bacteriophage MS2. *Mol. Pharmaceutics 10*, 69−76.

(21) Meldrum, T., Seim, K. L., Bajaj, V. S., Palaniappan, K. K., Wu, W., Francis, M. B., Wemmer, D. E., and Pines, A. (2010) A xenon-based molecular sensor assembled on an MS2 viral capsid scaffold. *J. Am. Chem. Soc. 132*, 5936−5937.

(22) Palaniappan, K. K., Ramirez, R. M., Bajaj, V. S., Wemmer, D. E., Pines, A., and Francis, M. B. (2013) Molecular Imaging of Cancer Cells Using a Bacteriophage-Based ^{129}Xe NMR Biosensor. *Angew. Chem. 125*, 4949−4954.

DOI: 10.1021/acs.bioconjchem.6b00275
Bioconjugate Chem. XXXX, XXX, XXX−XXX

(23) Tong, G. J., Hsiao, S. C., Carrico, Z. M., and Francis, M. B. (2009) Viral capsid DNA aptamer conjugates as multivalent cell-targeting vehicles. *J. Am. Chem. Soc. 131*, 11174−8.
(24) Wang, L., and Schultz, P. G. (2004) Expanding the genetic code. *Angew. Chem., Int. Ed. 44*, 34−66.
(25) Mehl, R. a., Anderson, J. C., Santoro, S. W., Wang, L., Martin, A. B., King, D. S., Horn, D. M., and Schultz, P. G. (2003) Generation of a bacterium with a 21 amino acid genetic code. *J. Am. Chem. Soc. 125*, 935−939.
(26) Francis, M. B., and Carrico, I. S. (2010) New frontiers in protein bioconjugation. *Curr. Opin. Chem. Biol. 14*, 771−773.
(27) Netirojjanakul, C., Witus, L. S., Behrens, C. R., Weng, C.-H., Iavarone, A. T., and Francis, M. B. (2013) Synthetically modified Fc domains as building blocks for immunotherapy applications. *Chem. Sci. 4*, 266−272.
(28) Mallikaratchy, P., Tang, Z., Kwame, S., Meng, L., Shangguan, D., and Tan, W. (2007) Aptamer directly evolved from live cells recognizes membrane bound immunoglobin heavy mu chain in Burkitt's lymphoma cells. *Mol. Cell. Proteomics 6*, 2230−2238.
(29) Stephanopoulos, N., Tong, G. J., Hsiao, S. C., and Francis, M. B. (2010) Dual-surface modified virus capsids for targeted delivery of photodynamic agents to cancer cells. *ACS Nano 4*, 6014−6020.
(30) Valegård, K., Liljas, L., Fridborg, K., and Unge, T. (1990) The three-dimensional structure of the bacterial virus MS2. *Nature 345*, 36−41.
(31) Schnurr, M., Witte, C., and Schröder, L. (2013) Functionalized ^{129}Xe as a potential biosensor for membrane fluidity. *Phys. Chem. Chem. Phys. 15*, 14178−14181.
(32) Bai, Y., Wang, Y., Goulian, M., Driks, A., and Dmochowski, I. J. (2014) Bacterial spore detection and analysis using hyperpolarized ^{129}Xe chemical exchange saturation transfer (Hyper-CEST) NMR. *Chem. Sci. 5*, 3197.
(33) Wang, Y., and Dmochowski, I. J. (2015) Cucurbit[6]uril is an ultrasensitive ^{129}Xe NMR contrast agent. *Chem. Commun. (Cambridge, U. K.) 51*, 8982−5.
(34) Zhou, X., Graziani, D., and Pines, A. (2009) Hyperpolarized xenon NMR and MRI signal amplification by gas extraction. *Proc. Natl. Acad. Sci. U. S. A. 106*, 16903−6.
(35) Kupce, E., Boyd, J., and Campbell, I. D. (1995) Short Selective Pulses for Biochemical Applications. *J. Magn. Reson., Ser. B 106*, 300−303.
(36) Shapiro, M. G., Ramirez, R. M., Sperling, L. J., Sun, G., Sun, J., Pines, A., Schaffer, D. V., and Bajaj, V. S. (2014) Genetically encoded reporters for hyperpolarized xenon magnetic resonance imaging. *Nat. Chem. 6*, 629−634.
(37) Wu, W., Hsiao, S. C., Carrico, Z. M., and Francis, M. B. (2009) Genome-free viral capsids as multivalent carriers for taxol delivery. *Angew. Chem., Int. Ed. 48*, 9493−9497.
(38) Stephanopoulos, N., Tong, G. J., Hsiao, S. C., and Francis, M. B. (2010) Dual-surface modified viral capsids for targeted delivery of photodynamic agents to cancer cells. *ACS Nano 4*, 6014−6020.
(39) Kunth, M., Witte, C., and Schröder, L. (2015) Continuous-wave saturation considerations for efficient xenon depolarization. *NMR Biomed. 28*, 601−606.

DOI: 10.1021/acs.bioconjchem.6b00275
Bioconjugate Chem. XXXX, XXX, XXX−XXX